



Research article

Dramatic change in the properties of magnetite-modified MOF particles depending on the synthesis approach

Lyubov Bondarenko^a, Rose Baimuratova^b, Marco Reindl^c, Verena Zach^c,
Artur Dzeranov^{a,b}, Denis Pankratov^d, Kamila Kydralieva^a,
Gulzhian Dzhardimalieva^{a,b}, Dagmar Kolb^{e,f,g}, Friedrich E. Wagner^h, Sebastian
P. Schwaminger^{c,g,*}

^a Moscow Aviation Institute (National Research University), Moscow, 125993, Russia

^b Federal Research Center of Problems of Chemical Physics and Medicinal Chemistry, Russian Academy of Sciences, Chernogolovka, Moscow Region, 119991, Russia

^c Division of Medicinal Chemistry, Otto-Loewi Research Center, Medical University of Graz, 8010 Graz, Austria

^d Department of Chemistry, Lomonosov Moscow State University, 119991, Moscow, Russia

^e Core Facility Ultrastructure Analysis, Center for Medical Research, Gottfried Schatz Research Center, Medical University of Graz, Graz, Austria

^f Division of Cell Biology, Histology and Embryology, Gottfried Schatz Research Center, Medical University of Graz, 8010 Graz, Austria

^g BioTechMed-Graz, 8010 Graz, Austria

^h Department of Physics, Technical University of Munich, James-Frank-Straße 1, 85748 Garching, Germany

ABSTRACT

Iron-containing metal–organic frameworks are promising Fenton catalysts. However, the absence of additional modifiers has proven difficult due to the low reaction rates and the inability to manipulate the catalysts. We hypothesize that the production of iron oxide NPs in the presence of a metal-organic framework will increase the rate of the Fenton reaction and lead to the production of particles that can be magnetically manipulated without changing the structure of the components. A comprehensive approach led to a metal organic framework using the example of MIL-88b (Materials of Institute Lavoisier) modified with iron oxides NPs: formulation of iron oxide in the presence of MIL-88b and vice versa. The synthesis of MIL-88b consists of preparing a complexation compound with the respective structure and addition of terephthalic acid. The synthesis of MIL-88b facilitates to control the topology of the resulting material. Both methods for composite formulation lead to the preservation of the structure of iron oxide, however, a more technologically complex approach to obtaining MIL-88b in the presence of Fe₃O₄ suddenly turned out to be the more efficient for the release of iron ions.

1. Introduction

Ferroptosis promises a novel potentially effective treatment strategy for cancer which is based on iron-dependent lipid peroxidation [1]. Many approaches focus on developing effective iron-containing preparations that can controllably induce reactive oxygen species (ROS). These Fenton reactions can cause cell death of cancer cells. The use of metal-organic frameworks (MOF), innovative porous materials consisting of metal ions or their clusters and connected to each other through organic linkers, can be a promising approach to release iron ions [2,3]. Their porosity is expressed by huge surface areas and can reach 7839 m²/g [4], and the drug payload can reach up to 25 mass% [5–7]. The undoubted advantage of MOF over other types of porous materials is the possibility of targeted construction of the network topology. This design creates conditions for the specific molecular interaction of a drug and a nanocarrier, and therefore

* Corresponding author. Division of Medicinal Chemistry, Otto-Loewi Research Center, Medical University of Graz, 8010 Graz, Austria.
E-mail address: sebastian.schwaminger@medunigraz.at (S.P. Schwaminger).

controlling the process of drug delivery [7–9]. However, the use of toxic raw materials in synthesis and the lack of proper purification technology significantly limit the biomedical use of these materials [10].

To obtain MOF, various synthetic approaches have previously been developed based on precipitation reactions at room temperature and under convective heating, including hydrothermal and solvothermal syntheses [11], and alternative routes based on other methods of introducing energy into the system are also used such as electrochemical [12,13], mechanochemical [14,15], microwave [16] and ultrasonic [17] radiation, as well as their combined effects [18]. It is known that when preparing MOFs containing mono- or hetero-metallic polynuclear clusters as an inorganic unit, it is difficult to select the conditions under which the target inorganic unit is formed “in situ” from inorganic salts [11]. For example, the use of ferric chloride and terephthalic acid in traditional solvothermal synthesis to obtain Fe-based MOFs can lead to the production of MIL-101(Fe), MIL-53(Fe), MIL-88B(Fe), etc. [19]. MOFs with trinuclear inorganic iron units already under visible light undergo direct excitation of Fe–O clusters and induce electron transfer from O^{2-} to Fe^{3+} , which subsequently affects the photocatalytic activity [20]. At the same time, the developed porous structure of MOF ensures effective diffusion of reagents to active iron centers. MIL-88B(Fe) is of greatest interest for catalytic transformations, including the Fenton reaction, since it has flexible behavior of the framework in the presence of polar solvents (for example, water), manifested in a change in the volume of its unit cell without loss of topology, which additionally improves the diffusion of reagents to active iron centers [21]. Moreover, electron-rich organic ligands of terephthalic acid typically act as electron donors for the reduction of Fe(III) to Fe(II) [22]. The low toxicity of Fe-based MIL materials was confirmed by both in vitro and in vivo toxicological studies. The safety and structural flexibility have promoted MIL-88B(Fe) to be used for drug delivery [23]. The use of pre-synthesized metal oxo-acetates [M3O(RCOO)6L3] ($M = Fe^{3+}$), including mixed valence, will probably allow us to consider the iron centers of MOFs not only as a structure-forming and transport link, but also as active centers capable of inducing ferroptosis by catalysis Fenton reactions. Coordination vacancy can be created upon the unsaturated Fe ions, which is beneficial for activating H_2O_2 [24]. Besides, its zeotype crystal structure endows it with well air, water and solvents resistance. Benefiting from these advantages, various MIL(Fe)-MOFs including MIL-88B [25], NH_2 -MIL-101Fe [26], and NH_2 -MIL-88B [27] have seen reports in heterogenous Fenton-like processes. But the results are inconsistent. For instance, for NH_2 -MIL-101Fe, $HO_2\cdot$ and $\cdot O^{2-}$ rather than $\cdot OH$ were reported to be the main ROS to degrade pollutants [28]. Dissolved iron ions in the solution could also react with H_2O_2 and generate $\cdot OH$ but with slower rate. For NH_2 -MIL-88B, it was reported that $\cdot OH$ and $\cdot O^{2-}$ are the dominant radicals in degradation [29]. Non-targeted ferroptosis induction can interfere with iron homeostasis and cause excessive ROS production, which can affect the immune system and cause neurodegenerative conditions such as Huntington’s and Parkinson’s disease, heart failure, and leukemia [30–34]. Therefore, it would be promising to create materials that would have synergistic properties: magnetic control and high catalytic activity of the Fenton reaction. There are different strategies to improve MIL-88b properties. Ye et al. [35] formulated MIL-88B(Fe)/ Fe_3S_4 hybrids with numerous and durable unsaturated iron sites, and S^{2-} ions acting as electron donors that enhanced the Fe(II) recycling in electro-Fenton (HEF) treatment of organic micropollutants at pH 7.0. Despite the quickest complete removal of trimethoprim at mild pH, only requiring 45 min, this particles cannot be controlled by magnetic field that which complicates their separation. Usman Akbar et al. [36] suggested to use multifunctional bimetallic (FeCo) bi-MIL-88B-FC MOFs modified with folic acid-conjugated chitosan as drug delivery systems (DDS) for targeted delivery of 5-Fluorouracil, but finally obtaining a bimetallic iron-cobalt alloy is time-consuming and cost process.

In our study we have selected Fe_3O_4 nanoparticles (NPs) as a magnetic material attached to the surface of the MOF or embedded inside the MOF. After introduction of the Fe_3O_4 NPs into MIL-88B(Fe), the magnetic MOFs should have superparamagnetic properties, so that the particles can be easily separated from the reaction mixture using an external magnetic field and also redispersed in the liquid phase after removal of the external magnetic field [37].

The aim of this work is to formulate iron-containing mesoporous materials that have the ability to induce ROS in high concentrations under model conditions. To obtain MIL-88b, a rational design for the preparation of MOF was used, which consisted of first preparing a complex compound that contains the required lattice unit (in this case, it is pre-synthesized trinuclear iron acetate), then the acetic acid residues were exchanged for the corresponding linkers that will connect these units in the lattice [38,39]. The advantage of this approach is the ability to control the topology of the resulting metal-organic framework, and, in general, the phase purity of the reaction product [40]. In search of the most gentle approaches to the synthesis of magnetite-modified MOF, we propose two production routes: formulation of iron oxide in the environment of pre-synthesized MOF (MOF- Fe_3O_4) and formulation of MOF in the presence of pre-synthesized magnetite (Fe_3O_4 -MOF). Thus, we have studied the microstructure, physicochemical characteristics, and the release of iron ions from MOF, Fe_3O_4 -MOF and MOF- Fe_3O_4 samples as an important Fenton-parameter for ferroptosis initiation.

2. Materials and methods

2.1. Chemicals and reagents

Ethanol and N, N-dimethylformamide (DMF) were purchased from RUSKHIM Chemicals Company (Moscow, Russia) and purified by distillation. Iron(III) chloride ($FeCl_3 \cdot 6H_2O$), sodium acetate ($CH_3COONa \cdot 3H_2O$), Iron(II) chloride ($FeCl_2 \cdot 4H_2O$) and terephthalic acid ($C_6H_4(CO_2H)_2$) was classified of at least as reagent grade and purchased from Sigma Aldrich. The water used in all experiments was deionized.

2.2. Preparation of MOF

The preparation of metal-organic framework (MOF) was carried out in two stages (Fig. 1). At the first stage complex compound which contains the necessary lattice node was synthesized. There is a trinuclear acetate block with the empirical formula $[Fe_3O$

$(\text{CH}_3\text{COO})_6(\text{H}_2\text{O})_3\text{Cl}\cdot 6\text{H}_2\text{O}$ ($\text{Fe}_3\text{OAcetate}$), then ligands of this node have been replaced by a terephthalic acid linker, which connected these nodes in the lattice.

Trinuclear acetate block synthesized according to the procedure described in the literature [41]. For synthesis $\text{FeCl}_3\cdot 6\text{H}_2\text{O}$ (24.33 g, 0.09 mol) was dissolved in 30 ml of hot water (50 °C). Sodium acetate (24.48 g, 0.18 mol) was dissolved separately in 30 mL of hot water (50 °C). The resulting solutions were mixed together and continued stirring at 50 °C for 25 min. The solution was left to cool in the air overnight for crystallization. After a few days, an orange-red powder was isolated on a Buechner funnel and washed with a small amount of cold ethanol. Then the precipitate was air dried to a constant mass for several days. Yield: 16.94 g (77%). Found (%): C, 19.5; H, 5.1; Fe, 23.1. Calculated for $[\text{Fe}_3\text{O}(\text{CH}_3\text{COO})_6(\text{H}_2\text{O})_3]\text{Cl}\cdot 6\text{H}_2\text{O}$ (wt%): C, 19.60; H, 4.93; Fe, 22.78; Cl, 4.82; IR (KBr -tablet), ν/cm^{-1} : 3523 ν (O–H); 2929 ν (CH); 1601, 1520 and 1444 ν COO; 1028; 664,599 ν (Fe–O).

For MOF synthesis terephthalic acid (5 g, 0.03 mol) and the $\text{Fe}_3\text{OAcetate}$ (7.35 g, 0.01 mol) were dissolved in 100 ml of DMF under stirring on a magnetic stirrer. The resulting mixture was boiled for 6–8 h under reflux at 153 °C until a dark red precipitate formed. The precipitate was isolated in a Buechner funnel, washed several times with fresh DMF, absolute ethanol and dried in vacuo (10^{-3} Torr, 80 °C, 10 h). Yield: 6.82 g (89%). Found (%): C, 36.72; H, 2.64; Fe, 21.6. Calculated for $[\text{Fe}_3\text{O}(\text{C}_8\text{H}_4\text{O}_4)_3(\text{H}_2\text{O})_3]\text{Cl}$ (wt%): C, 37.77; H, 2.37; Fe, 21.89; Cl, 4.63; IR (KBr -tablet), ν/cm^{-1} : 3420 ν (O–H); 2925 ν (CH); 1659,1578,1504 and 1391 ν COO; 748; 548 ν (Fe–O).

2.3. Preparation of the MOF- Fe_3O_4

In the first approach, magnetite NPs were synthesized in the presence of MOF by the Elmore reaction (eq. (4)) [43]:



For this purpose, 10.08 g (0.0373 mol) of $\text{FeCl}_3\cdot 6\text{H}_2\text{O}$ crystalline hydrate and 3.706 g (0.01864 mol) of $\text{FeCl}_2\cdot 4\text{H}_2\text{O}$ crystalline hydrate were dissolved in 200 mL of distilled H_2O in an argon atmosphere in the presence of 8 g of MOF. The solution was heated to 60 °C. With vigorous stirring, a 10% KOH solution was added to raise the pH to 10. The resulting MOF-magnetite precipitate was separated from the solution on a Büchner funnel by washing with pre-boiled hot (60–80 °C) distilled water, the sample was dried in vacuum (50 °C, 12 h). Yield: 4.68 g (39%). Found (%): C, 0.89; H, 0.96; Fe, 64.5. IR (KBr-tablet), ν/cm^{-1} : 3400 ν (O–H); 1619 and 1384 ν (COO); 1056; 548 ν (Fe–O).

2.4. Preparation of the Fe_3O_4 -MOF

In the second approach, MOF was synthesized in the presence of pre-synthesized Fe_3O_4 NPs. For this, on the first step magnetite was obtained by the Elmore reaction according to the 2.3 part in the absence of MOF. Further to 4 g of magnetite a solid terephthalic acid (5.90 g, 0.035 mol) and the $\text{Fe}_3\text{OAcetate}$ (8.70 g, 0.0118 mol) were added. The pH value was adjusted to 9 using a 10 M ammonia solution. The mixture was kept stirring on a mechanical stirrer for 30 min. The precipitate was purified in the same way as described in

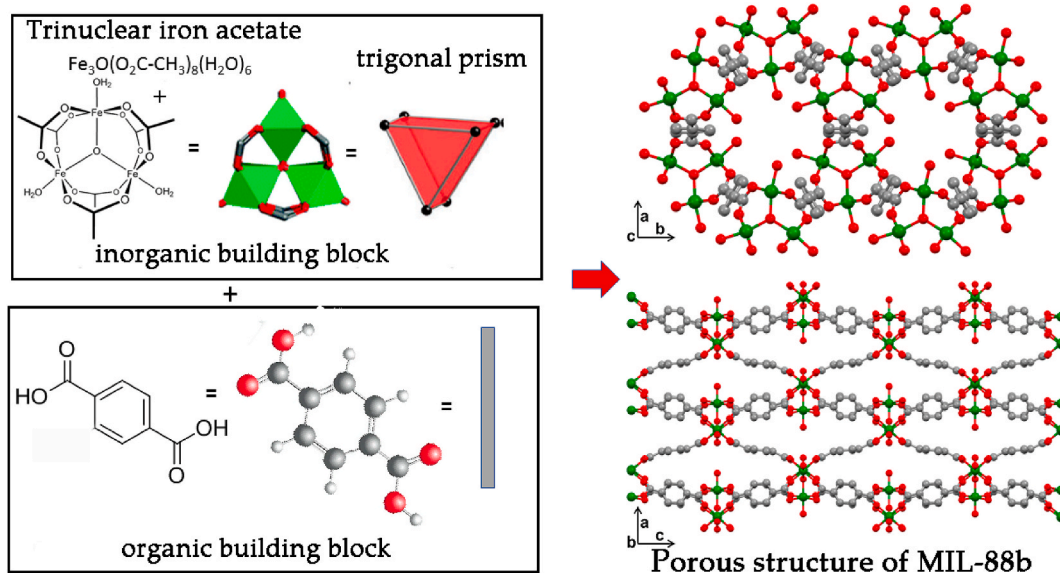


Fig. 1. Scheme of a metal-organic framework MIL-88b. On the left is secondary building units (SBUs) of MIL-88b. The ditopic terephthalate linker had abstracted as a rod, the $\text{Fe}_3\text{O}(\text{CO}_2)_6$ SBU as trigonal prism, and show their assembly into a 3D net (six-connected topology in which the node is a trigonal prism [42]). Hydrogen atoms have been left out for clarity. Fe: green, O: red, C: grey. (For interpretation of the references to colour in this figure legend, the reader is referred to the Web version of this article.)

the 2.2. Yield: 9.69 g (80 %). Found (%): C, 11.74; H, 2.72; Fe, 42.9. IR (KBr -tablet), ν/cm^{-1} : 3414 ν (O–H); 2930; 1632, 1558, and 1385 ν (COO); 1017; 583 ν (Fe–O).

2.5. Characterization of samples

X-ray diffraction (XRD) was performed in transmission geometry with a Stadi-P from STOE & Cie GmbH, Germany equipped with a MoK α source ($\lambda = 0.7093 \text{ \AA}$). The full width at half maximum (FWHM) of the all reflections was used for particle size determination with the Scherrer equation (Suppl, eq. S1). In order to quantify oxidation progress the (440) reflection was fitted with Voigt functions in Origin 2019 Pro (Suppl., eq S2).

The 440 reflection was fitted with a Voigt function with the software Origin in order to analyze the content of magnetite and maghemite based on the areas (A) of the respective reflections considering the following Equation (5):

$$\text{Fe}_3\text{O}_4 (\%) = 100 \frac{A(\text{Fe}_3\text{O}_4440)}{A(\text{Fe}_3\text{O}_4440) + A(\gamma\text{Fe}_2\text{O}_3440)} \quad (5)$$

Mössbauer spectra were measured in transmission geometry using an electromechanical velocity drive with a sinusoidal velocity waveform (Halder Elektronik, Germany) and a 25 mCi source of ^{57}Co in a rhodium matrix. The spectrometer was calibrated against $\alpha\text{-Fe}$ at ambient temperature. The 14.4 keV γ -rays were detected with a Kr proportional counter with single-channel analyzer windows set to the 14.4 keV photo-peak and the escape peak. For measurements at 4.2 K, the ^{57}Co -source and the absorber were cooled in a liquid helium bath cryostat. The Mössbauer spectra were approximated using the SpectRelax 2.8 software (Lomonosov Moscow State University, Russia). Isomeric shifts were converted relative to $\alpha\text{-Fe}$ at room temperature.

Raman spectroscopy was performed with a Raman Senterra spectrometer from Bruker Optics, Germany. Suspension drops had been deposited on microscope slides and dried under nitrogen atmosphere before spectra were recorded. A 488 nm laser was used and the laser power was reduced by optical filters to 0.1 mW for each measurement. In order to quantify the progress of oxidation, the A_{1g} band between 600 and 750 cm^{-1} was fitted with Voigt functions in Origin 2015 Pro.

The bands at 660 cm^{-1} and 710 cm^{-1} of MOF modified NPs (Fig. 6) were fitted with Voigt functions in Origin and used for magnetite content analysis (OriginLab Corporation, Wellesley, Massachusetts, US) (Fig. 6 c, d). The deconvolution was processed with Equation (6) in order to obtain the magnetite share [44].

$$\text{Fe}_3\text{O}_4 (\%) = 100 \left(1 - \frac{A(710)}{A(660)} \right) \quad (6)$$

The identification of functional groups and additional information on the type of coordination was carried out using FTIR spectroscopy (Spectrum 2, PerkinElmer, USA) with a spectral resolution of 2 cm^{-1} for the wavenumber range of 4000–350 cm^{-1} using a platinum attenuated total reflection device.

Scanning electron microscopy (SEM). Double sticky tape was placed on SEM stubs, and the particles were placed onto the stubs. Next, the samples were sputtered with a gold–palladium mixture at 10 nm thickness using a Bal-Tec SCD500 sputter coater. The particles were visualized using a Sigma 500 VP FE-SEM operated at 3 kV with a secondary electron detector.

Transmission electron microscopy (TEM). The morphology of the particles was evaluated using a Tecnai G2 20 transmission electron microscope (FEI Company, USA) operated at an accelerating voltage of 120 kV. Therefore, all samples were dissolved in distilled water using an ultrasonic processor (Fisherbrand, USA) at 75 % amplitude until a turbidity was visible by naked eye. 10 μL of each suspension was applied to carbon-coated copper grids (size 200 mesh) which had been pre-treated in a glow discharge cleaning system (PELCO Inc., USA). After an incubation for 1 min at room temperature, excessive liquid was gently removed by means of a filter paper. The TEM specimens were mounted in a TEM holder and analyzed subsequently. Images were acquired using a BM-Ultrascan 1000P CCD camera.

The magnetic properties of MNPs dry powders were characterized with a Vibrating Sample Magnetometer Lake Shore (Lake Shore Cryotronics, Westerville, OH, USA) at 300 K.

Textural characteristics of MNPs were measured using nitrogen adsorption/desorption isotherms at 77 K (liquid N_2) using a Quadrasorb SI setup (Quantachrome, USA) by the static volumetric method; samples were degassed by heating at 150 $^\circ\text{C}$ for 4 h under vacuum prior to analysis.

3. Results

3.1. Characterization

The purity of the resulting coordination polymer was confirmed by XRD (Fig. 3) and elemental analysis. To confirm the compliance of the obtained sample with the proposed structure, a diffraction pattern is presented in comparison with the calculated CCDC 2088535 (Suppl., Fig. S1) [45]. The coordination polymer is a MIL-88b-type framework having a hexagonal topology, in which the three-core iron cluster acts as a six-connected node with trigonal prism geometries. The elementary unit is a cluster compound, the metal centers of which are equivalent and each of them is octahedral bonded to six oxygen residues of terephthalic acid (Fig. 2).

It should be noted that the XRD profile of MOF after purification of dimethylformamide molecules with ethyl alcohol changes (Fig. 3a). This phenomenon is sometimes observed for flexible MOFs and called as « guest-responsive structural behavior » [46]. In our

system, it was shown that the coordination polymer exhibits a change in the orientation of the metal cluster and phenyl rings due to their rotation around the O–O axis of the carboxylate groups (knee-like axis of rotation) [47].

The crystalline structures of the MOF modified with Fe₃O₄ were identified with Rietveld refinement using Profex software (Fig. 3b, Suppl. Fig. 2S). The value goodness of fit for both samples was ~1.2. The lattice constants calculated from XRD are 8.378 Å and 8.373 Å for MOF-Fe₃O₄ and Fe₃O₄-MOF, respectively. According to ICDD-PDF 19–629, the characteristic peaks at 8.3, 13.7, 16.1, 19.5, 23.9, 25.9 and 27.7° corresponds to Fe₃O₄ phase in both samples. The broad peak at 4° in the sample can be attributed to MOF as the presence of carbon structure is further confirmed using FTIR spectroscopy and elemental analysis. The intensity of the peaks in the diffraction pattern indicates a higher content of the iron oxide phase in the MOF-Fe₃O₄ sample compared with the Fe₃O₄-MOF, where the MOF was obtained in the presence of magnetite. The results are consistent with the elemental analysis indicated 64.5 % and 42.9 % of Fe for MOF-Fe₃O₄ and Fe₃O₄-MOF respectively.

The crystallite size was estimated from XRD data with the Scherrer equation (Suppl., eq. S1). We used a spherical shape factor (0.89) and obtained smaller particle diameters than those measured manually on TEM images which is consistent with literature [80]. The diameter of NPs calculated by the Scherrer equation is 13.2 ± 3.8 nm for MOF-Fe₃O₄ and 12.6 ± 5.4 nm for Fe₃O₄-MOF, respectively.

Using XRD data-based approach from Kim et al. [48], which tried to differentiate between the distorted spinel of maghemite and the inverse spinel of magnetite in a powder XRD, we have deconvoluted the (440) reflection (Fig. 3c), which is a superposition of peaks at 27.59 ± 0.03° and 27.71 ± 0.03° for MOF-Fe₃O₄ and 27.61 ± 0.20° and 27.74 ± 0.11° for Fe₃O₄-MOF, respectively.

If we assume that the reflection angle corresponds to magnetite, and the peak larger reflection angle corresponds to maghemite, then the MOF-Fe₃O₄ contains 57.6% Fe₃O₄ and Fe₃O₄-MOF – 56.9% of Fe₃O₄, which indicates partial oxidation of magnetite during the synthesis of MOF.

Raman spectroscopy data allowing to recognize both MOF structural groups and iron oxide phase change are presented on Fig. 4. As showed on Fig. 4a, the bands of Raman spectra of MOF at 1612 cm⁻¹ were assigned to the COO⁻ asymmetric stretching vibration [49, 50]. The most prominent band (1612 cm⁻¹) is retained for samples modified with iron oxide, and a significant decrease in its intensity is associated with a decrease in the concentration of carbon and MOF in the end according to elemental analysis. The band at 634 cm⁻¹ is assigned to the in-plane bending of the carboxylate group OCO [51]. The medium band at 450 cm⁻¹ is assigned to the metal–oxygen bond [52]. Bands at 1427 cm⁻¹ and 1454 cm⁻¹ can be attributed to symmetric COO⁻ stretching vibrations in DMF and 1144 cm⁻¹ – to vibration of CH-group [50,53]. Previously, Schwaminger et al. [44,54] showed the interpretation of Raman spectra for iron oxide phase and great advantage of the analysis of Raman spectra for non-crystalline and extremely small particles. The oxidation of the divalent iron ions can be verified by the Raman mode (A_{1g}) near 660 cm⁻¹. For maghemite this mode is split into two equal components around 660 and 710 cm⁻¹ [55,56]. According to Ref. [57], the second mode refers to changes in the distance between Fe ions and O ions.

According to the calculations, the magnetite content in the magnetite-maghemite mixture is 0% for MOF-Fe₃O₄ and 14.4% for Fe₃O₄-MOF, which a bit differs from XRD data, but is in good agreement with Mössbauer data (Table 1, Figs. 5 and 6).

The Mössbauer spectrum at 4.2 K for the MOF sample is an intense symmetrical doublet against the background of a low-intensity sextet, somewhat broadened towards the inner part of the spectrum (Fig. 5). The experimental spectrum can be satisfactorily described by a model containing a superposition of two nested doublets with similar isomeric shifts, but differing in quadrupole splitting, and two nested sextets, which differ mainly in the values of the hyperfine magnetic field (Table 1). The hyperfine parameters of the doublets

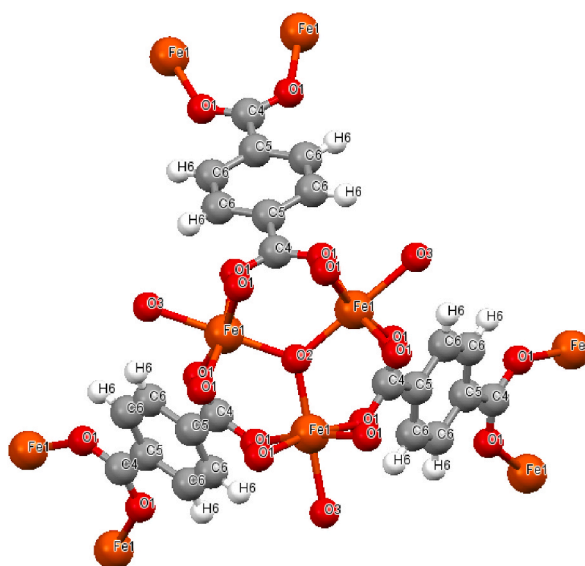


Fig. 2. Structure of the elementary unit of the coordination polymer Fe₃O(C₈H₄O₄)₃(H₂O)₃]Cl according to CCDC 2088535.

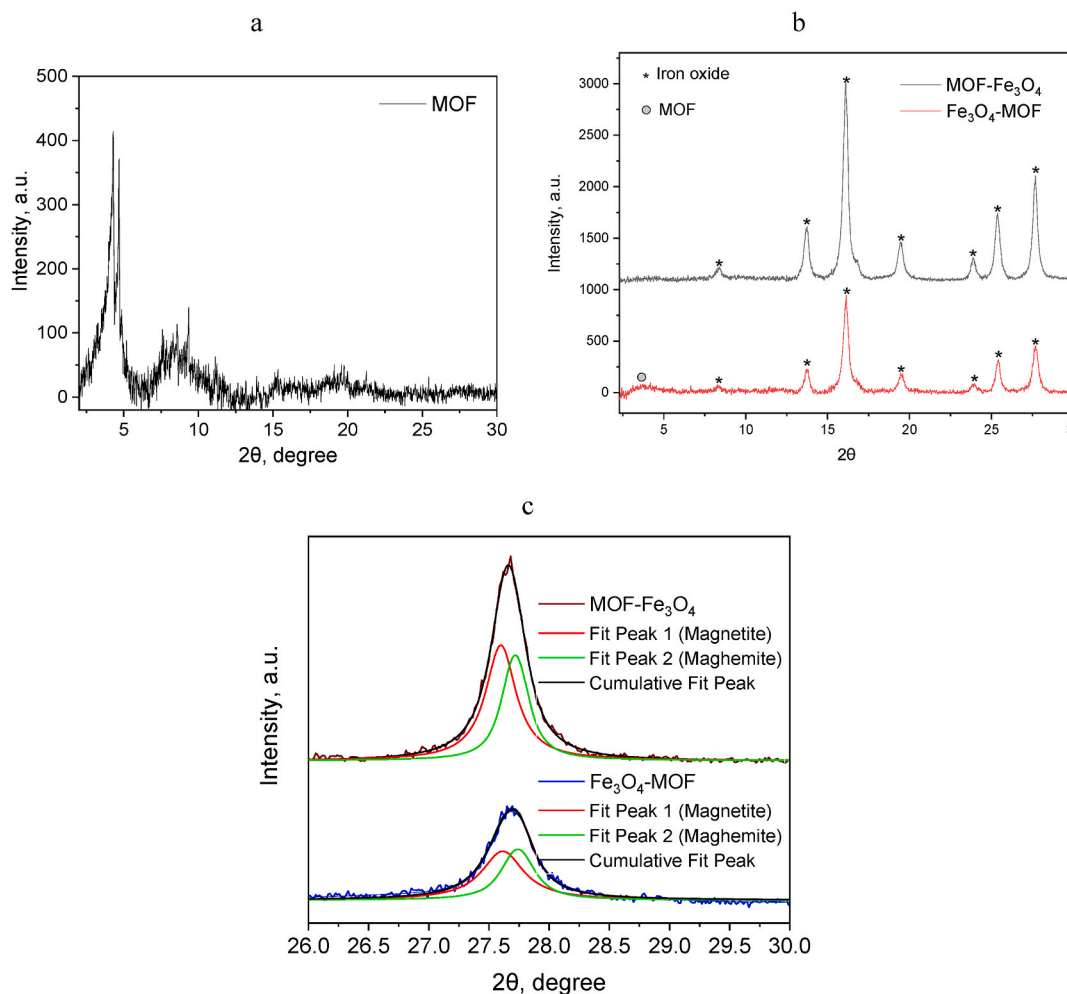


Fig. 3. XRD for MOF (a), MOF modified with Fe_3O_4 (b) and deconvolution of (440) peak of modified MOF (c) (R^2 0.99 and 0.98 for $\text{MOF-Fe}_3\text{O}_4$ and $\text{Fe}_3\text{O}_4\text{-MOF}$, respectively) (MoK α source ($\lambda = 0.7093 \text{ \AA}$)).

correspond to Fe^{3+} atoms in the high-spin state and octahedral environment [61–63]. The presence of sextets in the spectra may be due to the presence of impurities in the form of MOF hydrolysis products [64,65].

The Mössbauer spectra of the $\text{Fe}_3\text{O}_4\text{-MOF}$ and $\text{MOF-Fe}_3\text{O}_4$ samples at 4.2 K are asymmetric sextets with distorted resonance line profiles due to a noticeable broadening towards the inner region of the spectrum (Fig. 6). In this case, the width of the resonance lines and their distortions are noticeably higher in the case of the spectrum for the $\text{Fe}_3\text{O}_4\text{-MOF}$ sample compared to $\text{MOF-Fe}_3\text{O}_4$. This indicates the manifestation by the particles of the phenomenon of superparamagnetism, which is characteristic of nanosized particles, and the particle sizes of the $\text{Fe}_3\text{O}_4\text{-MOF}$ sample are smaller than the particle sizes of the $\text{MOF-Fe}_3\text{O}_4$ sample [66,67]. The features of the Mössbauer spectrum of the $\text{MOF-Fe}_3\text{O}_4$ sample include the presence of weak but clearly expressed resonant absorptions in the regions of -3 and 4 mm/s (Fig. 6) characteristic of magnetite, which can be caused by sextets of Fe^{2+} atoms in octahedral positions [68]. For the spectrum of the $\text{Fe}_3\text{O}_4\text{-MOF}$ sample, such features cannot be detected, possibly due to the high width of the resonance lines. Both spectra can be satisfactorily described by a set of 4 or 5 sextets ($\text{Fe}_3\text{O}_4\text{-MOF}$ and $\text{MOF-Fe}_3\text{O}_4$, respectively) whose profile is set within the many-state superparamagnetic relaxation model [69,70] (Table 1). In this case, within the framework of each sample, the relaxation spectra were related by a single relaxation time and the quotient of the magnetic anisotropy energy of the particles to the thermal energy:

$$\alpha = K V / k_B T, \quad (7)$$

where K is the magnetic anisotropy constant, V is the volume of the magnetic domain, k_B is the Boltzmann constant, T is the temperature [70]. On the whole, the obtained parameters (Table 1) agree with similar hyperfine parameters for low-temperature spectra of magnetite [68,71]. Analyzing the ratio $\alpha(\text{Fe}_3\text{O}_4\text{-MOF})/\alpha(\text{MOF-Fe}_3\text{O}_4)$ and assuming that the magnetic anisotropy constants for the samples are equal, one can easily show that the ratio of the linear dimensions of the magnetic domains is: $d(\text{Fe}_3\text{O}_4\text{-MOF})/d(\text{MOF-Fe}_3\text{O}_4) = 0.73$. Both spectra indicate no or just a very small amount of divalent iron ions. Assuming similarly [68] that subpeaks 4 and

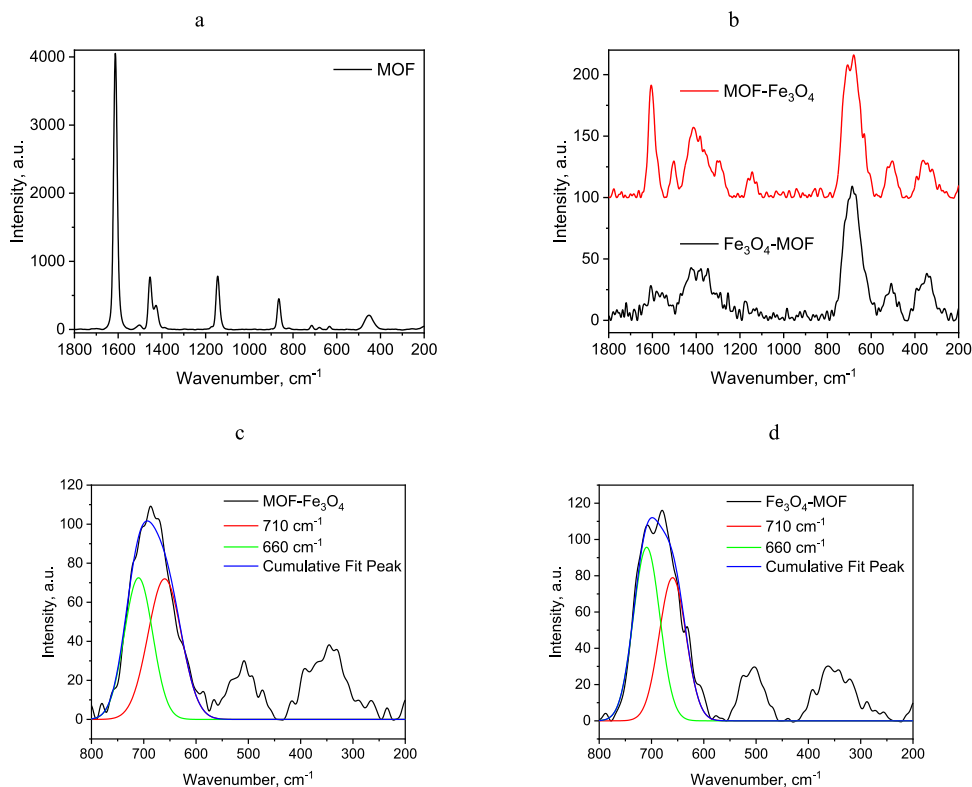


Fig. 4. Raman spectra of samples MOF (a) and MOF modified with Fe_3O_4 (b), which illustrate the deconvolution fitting of MOF- Fe_3O_4 (c) and Fe_3O_4 -MOF (d).

Table 1

^{57}Fe Mössbauer parameters for the samples at 4.2 K.

Sample	N^{\square}	δ^a , mm/s	Δ , mm/s	Γ_{exp} , mm/s	H_{eff} , kOe	$\alpha = KV/k_B T$	S, %
MOF	1	0.50	-0.06	0.87	489.3		19.2
	2	0.46	-0.02	1.01	448		15.1
	3	0.54	0.58	0.38			35
Fe_3O_4 -MOF	4	0.57	0.77	0.71			30.9
	1	0.52	-0.03	0.34	543.0	8.20	36
	2	0.40	0.14	0.32	528.9		22
MOF- Fe_3O_4	3	0.42	-0.17	0.54	515.5		35
	4	0.78	0.06	0.31	501.1		7.3
	1	0.51	-0.03	0.39	542.7	20.7	36.3
	2	0.40	0.14	0.34	529.4		23.1
	3	0.46	-0.11	0.46	518.9		37
	4	1.10	-0.41	0.60	467.0		2.6
	5	0.90	0.90	0.60	380.0		1.3

^a δ — the isomeric shift, Δ — the quadrupole splitting, Γ_{exp} — the linewidth, H_{eff} — the hyperfine magnetic field, S — the relative area of the subspectrum, α — the quotient of particle anisotropy energy to thermal energy as (7).

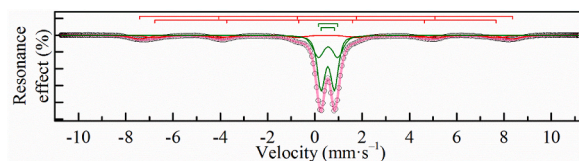


Fig. 5. Mössbauer spectrum at 4.2 K of a MOF sample.

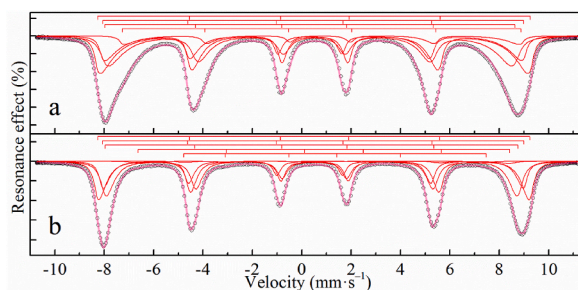


Fig. 6. Mössbauer spectra at 4.2 K of Fe_3O_4 -MOF (a) and $\text{MOF-Fe}_3\text{O}_4$ (b) samples.

5 refer to Fe^{2+} atoms in the octahedral positions of spinel, and assuming that the areas of the subspectra are proportional to the content of iron atoms in the corresponding states, the ratio of iron ions can be calculated as [72]:

$$X_{ms} = \frac{\text{Fe}^{2+}}{\text{Fe}^{3+}} = \frac{S4 + S5}{S1 + S2 + S3}, \quad (8)$$

where $S\#$ – area of subspectrum $\#$. From the resulting relationship it is easy to estimate the nonstoichiometry parameter of magnetite - δ [73]:

$$\delta = \frac{1 - 2X_{ms}}{3 + 2X_{ms}}. \quad (9)$$

Thus, from the experimental data of Mössbauer spectroscopy, the nonstoichiometry parameter δ for $\text{Fe}_{3-\delta}\text{O}_4$ -MOF and $\text{MOF-Fe}_{3-\delta}\text{O}_4$ can be estimated as 0.2668 ± 0.0024 and 0.2982 ± 0.0009 , respectively. This indication is in good agreement with the Raman spectra which also indicate an oxidation of the iron oxide particles.

Fourier transform infrared spectrophotometry (FTIR) was used also for quantification of magnetite and maghemite phase. In accordance with the IR spectroscopy data presented in Fig. 7, MOF demonstrates broad absorption bands in the range of $2800\text{--}3600\text{ cm}^{-1}$, which correspond to the stretching vibrations of OH-groups of both physically adsorbed and crystallized water molecules.

Stretching vibrations of the C-H group in terephthalic acid molecules appear in the spectrum at $2950\text{--}2640\text{ cm}^{-1}$ with a maximum intensity at 2925 and 2855 cm^{-1} , which is also absent on the surface. Asymmetric and symmetric stretching vibrations of the COO^- carboxyl group are observed at $1580\text{--}1565$ and $1444\text{--}1378\text{ cm}^{-1}$. Since the nature of carboxylate coordination can be judged from the difference between $\nu_{\text{as}}(\text{COO}^-)$ and $\nu_{\text{s}}(\text{COO}^-)$, it is assumed that the carboxylate ion is coordinated with the metal cation in the bidentate coordination mode ($\Delta\nu \leq 187\text{ cm}^{-1}$) according to the literature data [52,58]. The metal-oxygen (Fe-O) vibration band is present in the region of 548 cm^{-1} and, according to compassion of bond's squares, 47.6% of Fe-O are located on the surface.

The functionalization of MOF leads to a decrease in the intensity of the bands related to the presence of water in the samples (region $\sim 3400\text{ cm}^{-1}$) by 20% sequentially when obtaining MOF in the presence of magnetite and by 50% when obtaining magnetite in the presence of MOF (Fig. 7). In addition, both approaches to the preparation of the nanocomposite led to a decrease in the intensity of the C=O bands by 85% and 92% for Fe_3O_4 -MOF and $\text{MOF-Fe}_3\text{O}_4$, respectively, in comparison to MOF, which is confirmed by elemental analysis data.

Namduri et al. [59] using FTIR spectroscopy data for quantification of magnetite and maghemite phases in multi-component

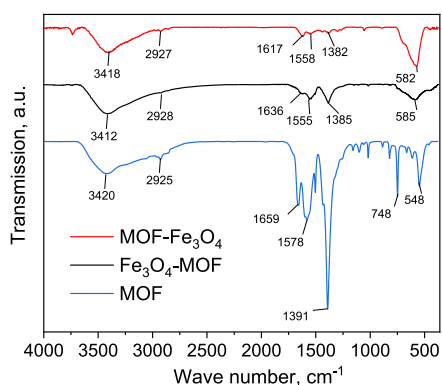


Fig. 7. FTIR spectra for MOF, $\text{MOF-Fe}_3\text{O}_4$ and Fe_3O_4 -MOF.

unknown sample showed that FTIR spectrum of magnetite exhibits two strong infrared absorption bands at 570 cm^{-1} (t1, mode of the tetrahedral and octahedral sites according to Ref. [60] and 390 cm^{-1} (t2). Maghemite has absorption bands at 630 cm^{-1} , 590 cm^{-1} , and 430 cm^{-1} . Thus, the 570 cm^{-1} and 630 cm^{-1} bands, respectively, can be considered the most intense characteristic bands of magnetite and maghemite. The deconvolution of the bands 582 cm^{-1} for MOF- Fe_3O_4 and 585 cm^{-1} for Fe_3O_4 -MOF showed that the bands contained in them can be attributed to magnetite ($568.25 \pm 1.74\text{ cm}^{-1}$ for MOF- Fe_3O_4 and $569.70 \pm 8.26\text{ cm}^{-1}$ for Fe_3O_4 -MOF) and maghemite ($626.69 \pm 3.12\text{ cm}^{-1}$ for MOF- Fe_3O_4 and $613.72 \pm 14.54\text{ cm}^{-1}$ for Fe_3O_4 -MOF) (Fig. 8).

The size change of MOFs after functionalization with magnetite was evaluated using TEM and SEM. According to the data of SEM micrographs (Figs. 9 and 10), MOF agglomerates of the MIL-88b type have the shape of an elongated hexagonal bipyramid or rod-like shape, which is often found in the previous research [74–76]. According to statistical processing, the length of the MOF particles was $12.27\text{ }\mu\text{m} \pm 2.89\text{ }\mu\text{m}$ (Fig. 9c), and the width was $3.84\text{ }\mu\text{m} \pm 1.13\text{ }\mu\text{m}$ (Fig. 9d), which correlates with the dimensions of MIL-88b obtained in other studies. Thus, Gao et al. [74], reported about the MOF length of 6–8 μm and the particle diameter of 4 μm , and Wang et al. [75], report about the MOF length of 2.8 μm and the particle diameter of 12 nm.

Functionalization with magnetite leads to a dramatic change in the morphology of the samples. Thus, for MOF- Fe_3O_4 samples (Fig. 10 a), the morphology is close to the morphology of non-functionalized magnetite, which represents spherical particles. Moreover, elemental analysis data also confirms practically no MOF into MOF- Fe_3O_4 sample according to content of C ca. 1 %, which is consistent with our and other data [77–79]. The probable reasons for the destruction of MOFs during synthesis are discussed in the discussion section. At the same time, the Fe_3O_4 -MOF (Fig. 10 c, d) sample demonstrates a significant change in the morphology of the MOF from pyramidal to lamellar, probably associated with the limitation of the growth of the MOF along one of the magnetite planes.

A decrease in the concentration of MOF in the sample naturally led to a decrease in the specific surface area (SSA) from $220.2\text{ m}^2/\text{g}$ for MOF to $197.8\text{ m}^2/\text{g}$ for Fe_3O_4 -MOF and $127\text{ m}^2/\text{g}$ for MOF- Fe_3O_4 (Table 2). The SSA and the pore diameter of samples determined by N_2 absorption–desorption technique using Brunauer-Emmett-Teller and Barrett-Joyner-Halenda methods, respectively are presented in Table 2.

The SSA for the MOF made $220.2\text{ m}^2/\text{g}$ and an average pore diameter of 3.59 nm. The preparation of magnetite in the presence of MOF led to a significant decrease in the surface area to $127.3\text{ m}^2/\text{g}$, which may be associated with the destruction of MOF under strongly alkaline conditions of synthesis that confirmed by elemental analysis (0.93% C in the MOF- Fe_3O_4 sample). On the other hand, the preparation of MOF in the presence of magnetite (Fe_3O_4 -MOF) slightly reduced in compare with native MOF the surface area to $197.8\text{ m}^2/\text{g}$ at C content of 11.74 %. Interestingly to note, that this method of preparation led to an increase in average pore diameter to 8.74 nm.

The most crucial property of MNPs, which allow a variety of applications, especially in biomedicine, is represented by their ferrimagnetism. As a matter of fact, the application of an external magnetic field makes it possible to concentrate magnetic NPs in the target point, thus reducing likely side effects of iron release. The hysteresis loops for the three different MNPs samples were closed and symmetrical with respect to the origin of the coordinate system as reported in Fig. 12. The shape of the loops indicates the ferrimagnetic features of the material which are prone to their potential application.

Some magnetic characteristics for the magnetite-modified MOF NPs are presented in Table 3. The saturation magnetization σ_s of MOF- Fe_3O_4 and Fe_3O_4 -MOF samples were respectively 49.9 and 18.6 emu g^{-1} (Table 3), which is consistent with 62.4 and 42.9% of Fe content respectively according to elemental analysis. The determined saturation magnetization σ_s values indicate that NMPs exhibit superparamagnetic properties at room temperature.

In the absence of a magnetic field, all samples showed a similar low residual magnetism $\sim \pm 1\text{--}3\text{ emu g}^{-1}$ (Table 3) due to magnetic viscosity for superparamagnetic materials [81]. In general, the magnetite-modified MOF MNPs exhibit a saturation magnetization sufficient to control an external magnetic field. For biomedical applications such as drug delivery and hyperthermia a saturation magnetization of $\sim 8\text{--}19\text{ emu g}^{-1}$ is required which according to vibrating-sample magnetometry results the synthesized multifunctional magnetite mesoporous silica nanoparticles coated with a chitosan hydrogel are useful for biomedical applications [82–84]. In

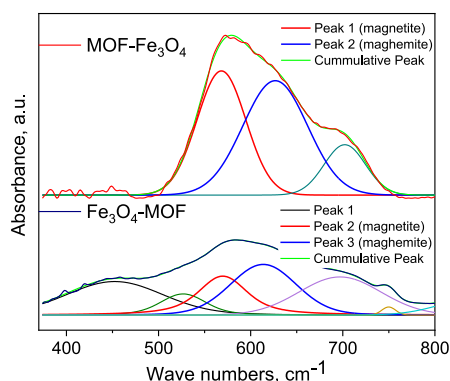


Fig. 8. IR-spectra for MOF- Fe_3O_4 and Fe_3O_4 -MOF samples: deconvolution fitting for bond 582 cm^{-1} for MOF- Fe_3O_4 and 585 cm^{-1} for Fe_3O_4 -MOF.

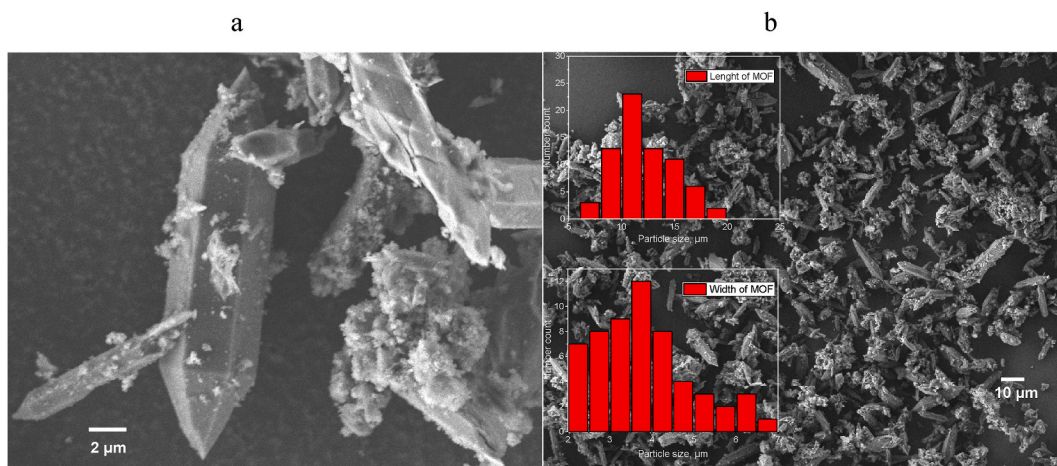


Fig. 9. SEM images of MOF at 2 μm (a) and 10 μm (b) resolution, size distribution for MOF length and width (In order to receive statistical particle distributions at least 100 particles were counted per picture; at least three pictures were used for each calculation).

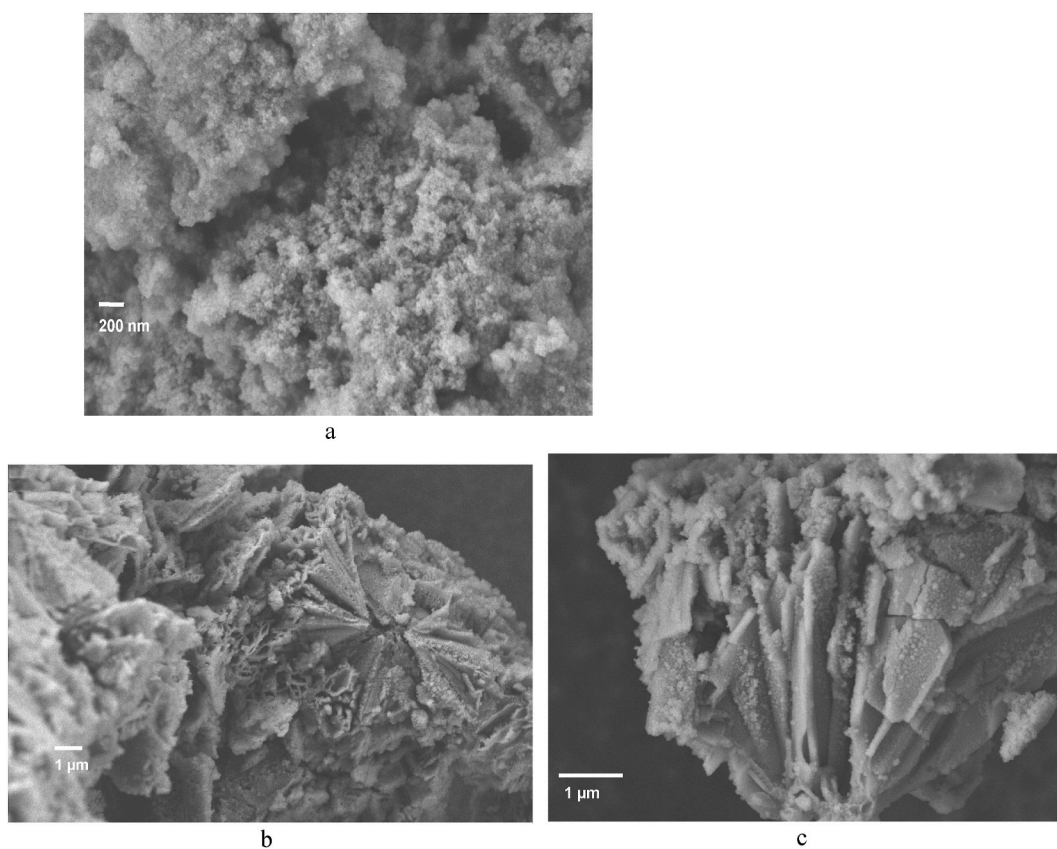


Fig. 10. SEM of MOF-Fe₃O₄ (a) and Fe₃O₄-MOF(c,d) Besides counting of particle diameters from TEM micrographs (Fig. 11).

many works focused on the preparation of materials for catalyzing ferroptosis the authors have used iron salts as iron ions sources [29, 91, 92]. However, as reported by Huo et al. in Ref. [85], without targeting only 6.95% of MNPs were stored and localized in the 4T1 cancer cell 48 h upon injection.

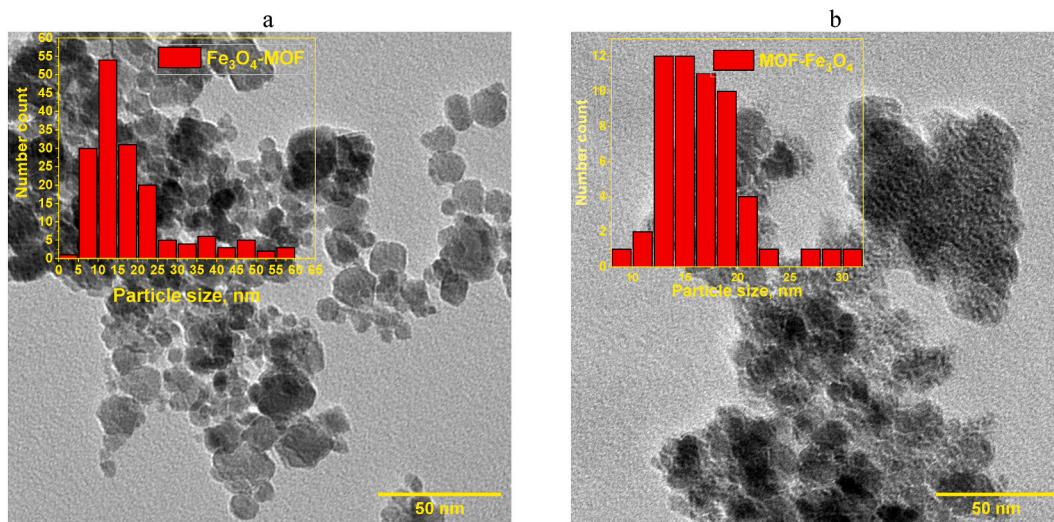


Fig. 11. TEM images of samples: (a) for Fe_3O_4 -MOF with particles distribution; for MOF- Fe_3O_4 (b) with particles distribution (In order to receive statistical particle distributions at least 100 particles were counted per picture; at least three pictures were used for each calculation).

Table 2

Specific surface area and pore size of samples.

	S_{BET} , m^2/g	V(BET) pore for $P/P_0 = 0.99$, cm^3/g	BJH	
			V, cm^3/g	d, nm
MOF	220.2	0.32	0.25	3.59
MOF- Fe_3O_4	127.3	0.27	0.23	3.61
Fe_3O_4 -MOF	197.8	0.29	0.27	8.74

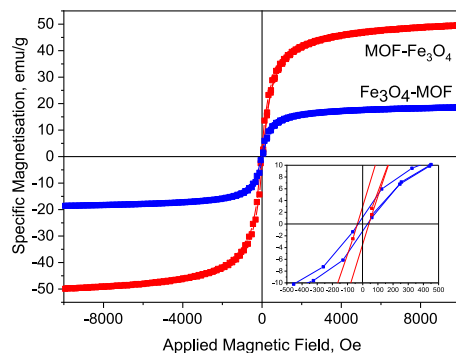


Fig. 12. Magnetization curves (room temperature) for MOF modified with Fe_3O_4 .

Table 3

Magnetic properties of samples MOF modified with Fe_3O_4 .

Sample	σ_s , $\text{G}\cdot\text{cm}^3\text{g}^{-1}$	σ_r , $\text{G}\cdot\text{cm}^3\text{g}^{-1}$	H_c , Oe
MOF- Fe_3O_4	49.9	3.00	35
Fe_3O_4 -MOF	18.6	1.17	31

4. Discussion

In this study, the functionalization of MOF with magnetite NPs was carried out to magnetize MOF, which will allow to control the material when exposed to an external magnetic field. In order to select conditions for maximum preservation of the structure and properties of the magnetic complex, this study used two approaches to the functionalization of a known coordination polymer MIL 88B (Fe) with magnetite Fe_3O_4 : (i) by synthesizing magnetite in the presence of pre-synthesized MOF, and vice versa, (ii) by synthesizing MOF in the presence of pre-synthesized magnetite. Both MOFs and magnetite NPs are known to be sensitive to reaction conditions. For example, magnetite NPs are easily oxidized to maghemite [86], which leads to a decrease in saturation magnetization. Thus, in this study, the state of magnetite and MOF was monitored using different methods to obtain a reliable picture of the structure of the components. Control over the preservation of magnetite was carried out by assessing the percentage of magnetite in both synthesis approaches using X-ray phase analysis, Mössbauer spectroscopy and Raman spectroscopy. The use of various methods to quantify magnetite is justified by the following. While distinguishing between magnetite and maghemite from XRD is quite difficult [48], in Mössbauer spectroscopy, divalent and trivalent iron ions can easily be distinguished due to different isomer shifts [68]. With Raman spectroscopy, magnetite and maghemite NPs can even be accurately differentiated at room temperature. Different phonon modes exist for the inverse spinel configuration of magnetite and the defect spinel structure of maghemite which correspond to different Raman shifts [87,88].

Comparative analysis of magnetite content in magnetic MOF complexes using different methods is presented on Fig. 13.

Thus, the preparation of magnetite in the presence of MOF (MOF- Fe_3O_4) leads to the complete oxidation of Fe^{2+} ions to Fe^{3+} ions, while Mössbauer spectroscopy data indicate partial retention of Fe^{2+} ions in the core of the sample MOF- Fe_3O_4 . The approach to synthesis of MOF particles in the presence of magnetite NPs (Fe_3O_4 -MOF) makes it possible to partially retain Fe^{2+} ions both on the surface and in the core of the sample Fe_3O_4 -MOF leads to particles in a transition state between magnetite and maghemite. This is in good accordance with previous findings [54]. The difference in results may be explained by differences in the nature of the analysis methods used. With Mössbauer spectroscopy one can see the oxidation of the iron ions before the whole crystal changes. With Raman, one observes slightly different distances between iron ions and oxygen ions and with XRD one observes the oxidation at last when everything is completely reoriented in a new lattice. In general, both existing phases of the magnetite-maghemite mixture in both samples allow them to be successfully used to control the magnetic field.

Regarding MOF structure, we observe more significant changes in the two synthesis approaches. Heterogeneous MOF systems are capable to degrade in aggressive environments [89]. Degradation is also important for selecting conditions for the synthesis of composite materials with MOFs. The very low content of MOF (according to 1 % C) into MOF- Fe_3O_4 , i.e. during synthesis in situ for magnetite NPs (MOF- Fe_3O_4) was a reason to for further study. To study the stability of MIL-88B in different media, buffer solutions were prepared: acetate buffer with pH 4.6 and phosphate buffer with pH 8. The degree of MOF decomposition was determined using a UV spectrometer (SPECS-SSP-705-1 spectrometer, JSC Spectroscopic Systems, Moscow, Russia) based on the peak intensity of 238 nm, corresponding to the electronic transitions of the benzene ring of terephthalic acid (TPA). To calculate the true concentration of TPA, a calibration graph was constructed (Fig. 14). The solubility of TPA is low, so it was converted to the potassium form to obtain calibration dependences. Preliminary studies have shown that conversion to this form does not affect the extinction of the benzene ring. The samples were also kept in distilled water with a resulting pH of 5.6, 5, 15, or 25 mg of synthesized MOF were placed in 10 g of the test medium. The tubes were mixed with a shaker for the first 90 min, then centrifuged at 1100 rpm, and the mother solution was examined using UV. When studying the mother liquor in phosphate buffer, the filtrate was subjected to a 10-fold dilution due to high concentrations of TPA. The degree of MOF degradation was determined based on the percentage of TPA in the structure. The stability of the synthesized MOF (MIL-88B) was studied at three pH values.

When MOF is kept in distilled water with pH = 5.6 for two days, no significant increase in TPA concentration is observed (Fig. 15e).

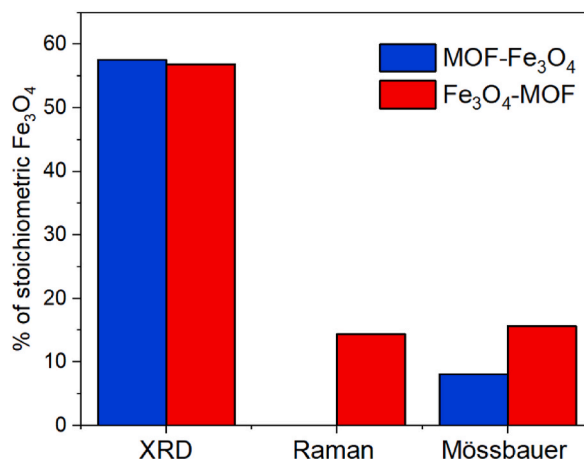


Fig. 13. Comparison of % of stoichiometric Fe_3O_4 for different samples.

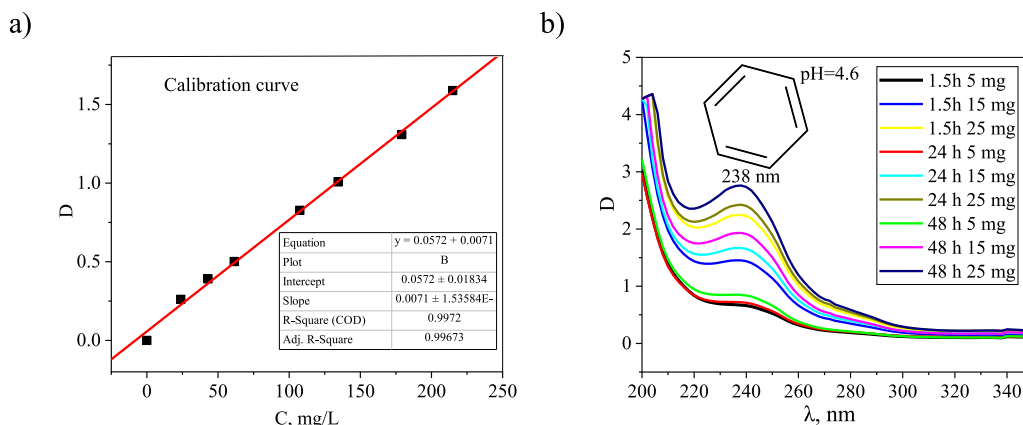


Fig. 14. Calibration curve for determining the content of TPA in an aqueous solution (a); UV spectra of solutions after centrifugation at different times and MOF concentrations at pH = 4.6.

The concentration of TPA released from MOF is practically independent of the mass of the initial sample; the maximum release is observed after 1.5 h of exposure. Apparently, in this case, there is an equilibrium release of unreacted TPA physically adsorbed in the pores. At acidic pH (4.6), a release of TPA equivalent to the weight of the sample used is observed (Fig. 15c). 20% of MOF is destroyed already at 2 h of exposure, then the degradation process slows down, but continues. A similar effect was discovered during the study for NH₂-MIL-88B(Fe) in the pH range from 3.0 to 11.0; the critical value turned out to be pH = 5.0, above which the number of released iron ions tended to zero, and when moving towards more acidic pH, iron ions were actively released [22]. The influence of the alkaline environment appears to be significant on the synthesized MIL-88b. Thus, it was demonstrated that MOF degrades by 80% already in the first 1.5 h of exposure to phosphate buffer (Fig. 2d). A similar effect on degradation was observed when studying the degradation mechanism of two different iron carboxylate MOFs, MIL-100 (Fe) and MIL-53 (Fe) [90]. The authors observed the formation of α -Fe₂O₃ and hematite at elevated temperatures or after changes in pH above 7. The release curves at high concentrations of TPA in an alkaline medium do not show a dependence on the sample weight (above 15 mg), partly this behavior can be explained by the poor solubility of TPA in aqueous media and achieving an equilibrium soluble concentration.

Thus, at alkaline pH, significant degradation of MOFs is observed, releasing linkers. This process results in incomplete inclusion of MOF in the synthesis with in situ obtained magnetite NPs (MOF-Fe₃O₄). This highlights the importance of in-depth study of the degradation of each type of MOF under different experimental conditions to develop approaches for preparing composite materials.

4.1. Potential application as ferroptosis initiators

To understand the prospects of using these NPs as ferroptosis initiators, we preliminarily studied the concentration of ions released into the solution from the surface/volume of NPs at pH 4.5. UV-Vis spectroscopy was used to demonstrate the kinetics and concentration of the released Fe²⁺ and Fe³⁺ from MOF, Fe₃O₄-MOF, MOF-Fe₃O₄ (see Supplementary Materials, Fig. S2). The concentrations of iron ions were recalculated per 1 g of the iron. Since the Fenton reaction is a disproportionation reaction of hydrogen peroxide (H₂O₂) with further production of a highly reactive hydroxyl radical •OH (E₀ = 2.80 V), the release of Fe²⁺ and Fe³⁺ was evaluated in the absence/presence of hydrogen peroxide to assess the selectivity of the NPs used (since tumor cells are characterized by an increased content of H₂O₂).

According to Fig. 16 a,b, MOF releases the highest concentration of both Fe³⁺ and Fe²⁺ reaching 12% and 7%, respectively, of the total amount of iron 60 min after the start of measurements. The evaluation was carried out only for iron ions in solution, without taking into account surface iron ions. Functionalization with magnetite leads to a significant decrease in the concentration of released ions to (maximally) 1.3% of Fe³⁺ and 0.1% of Fe²⁺ for MOF-Fe₃O₄ (Fig. 16 c, d) and 2.7% of Fe³⁺ and 0.5% of Fe²⁺ for Fe₃O₄-MOF (Fig. 16 e, f). A significant decrease in the concentration of ions can be associated with a decrease in the concentration of MOFs in the composition of NPs after functionalization to 0.9% and 33.6% for MOF-Fe₃O₄ and Fe₃O₄-MOF, while the difference in ions concentration between magnetic composites can also be due to a high content of iron (64.5 %) for the Fe₃O₄-MOF sample as compared to the iron concentration in the MOF-Fe₃O₄ (42.9%).

5. Conclusion

In this work, magnetic materials based on the MIL88b metal-organic framework modified with magnetite were synthesized by two approaches: the preparation of magnetite in the presence of MOF and the preparation of MOF in the presence of magnetite. Analysis of the microstructure and comparison of the results of XRD, Raman and Mössbauer spectroscopy showed that both iron oxide-containing samples are a mixture of two iron oxides, magnetite and maghemite. It has been shown that the production of magnetite in the presence of MOF (MOF-Fe₃O₄) leads to the complete transformation of magnetite into maghemite on the nanoparticle surface, while the

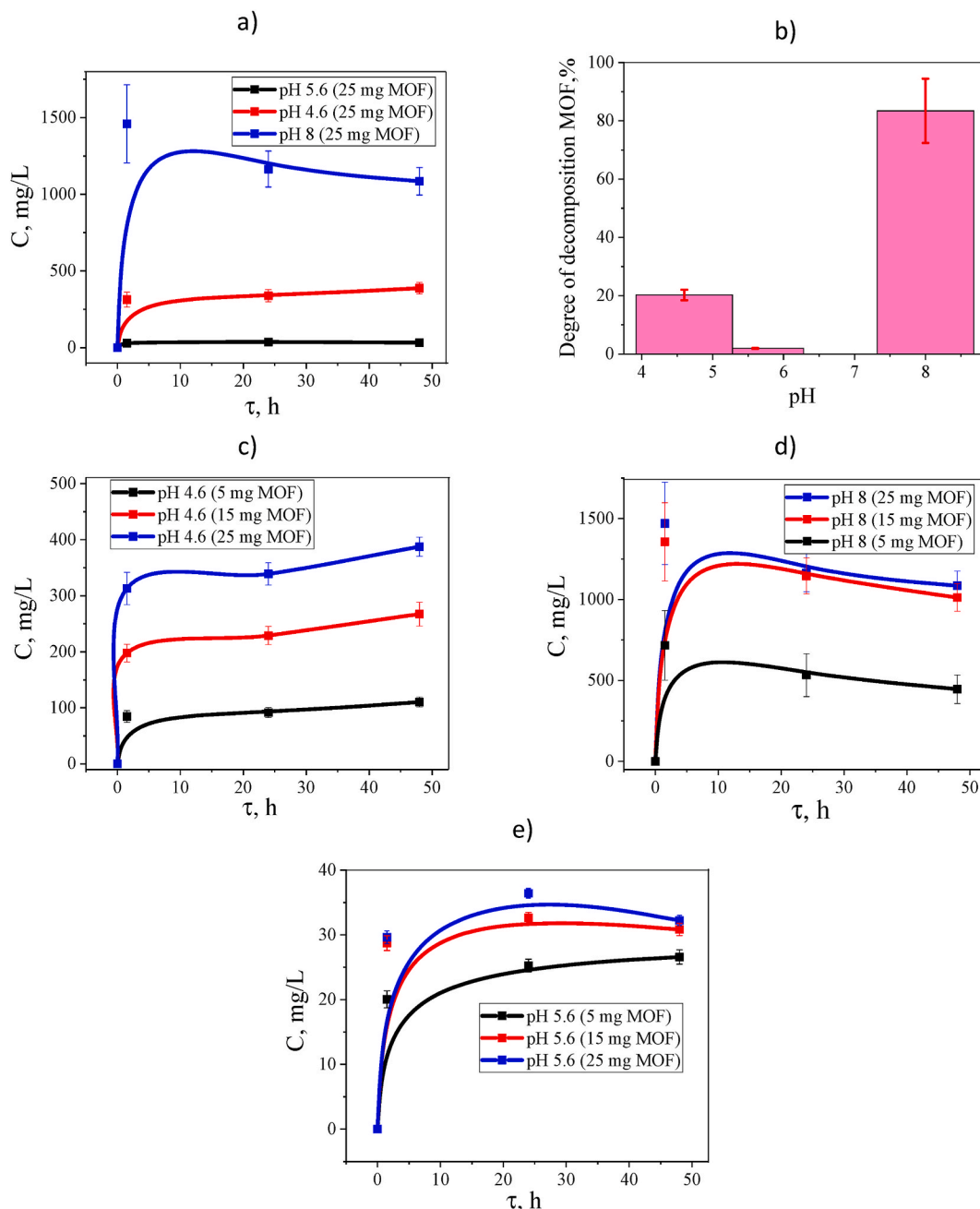


Fig. 15. Concentration of released TPA at different pH upon degradation of MOF (MIL-88b) with different masses (a, c, d, e); and degree of degradation of MOF after 90 min of treatment (b).

production of MOF in the presence of magnetite ($\text{Fe}_3\text{O}_4\text{-MOF}$) allows partial retention of Fe^{2+} ions both on the surface and in the core of the sample. The presence of Fe^{2+} ions should favorably affect the rate of the Fenton reaction, which will be assessed in our next work. Also the preparation of MOF in the presence of magnetite ($\text{MOF-Fe}_3\text{O}_4$) leads to the production of materials with a high content of MOF in the composition (11.74% C for $\text{Fe}_3\text{O}_4\text{-MOF}$ compared to 0.93% for $\text{MOF-Fe}_3\text{O}_4$). A dramatic decrease in the concentration of MOF occurred due to the destruction of the metal-organic framework under alkaline conditions, which was shown by us. A preliminary assessment of the samples as sources of iron ions for initiating the Fenton reaction showed that the most promising materials are samples with a high content of MOF and Fe^{2+} ions (MOF and $\text{Fe}_3\text{O}_4\text{-MOF}$). The application of these samples in the Fenton reaction is object for our future research.

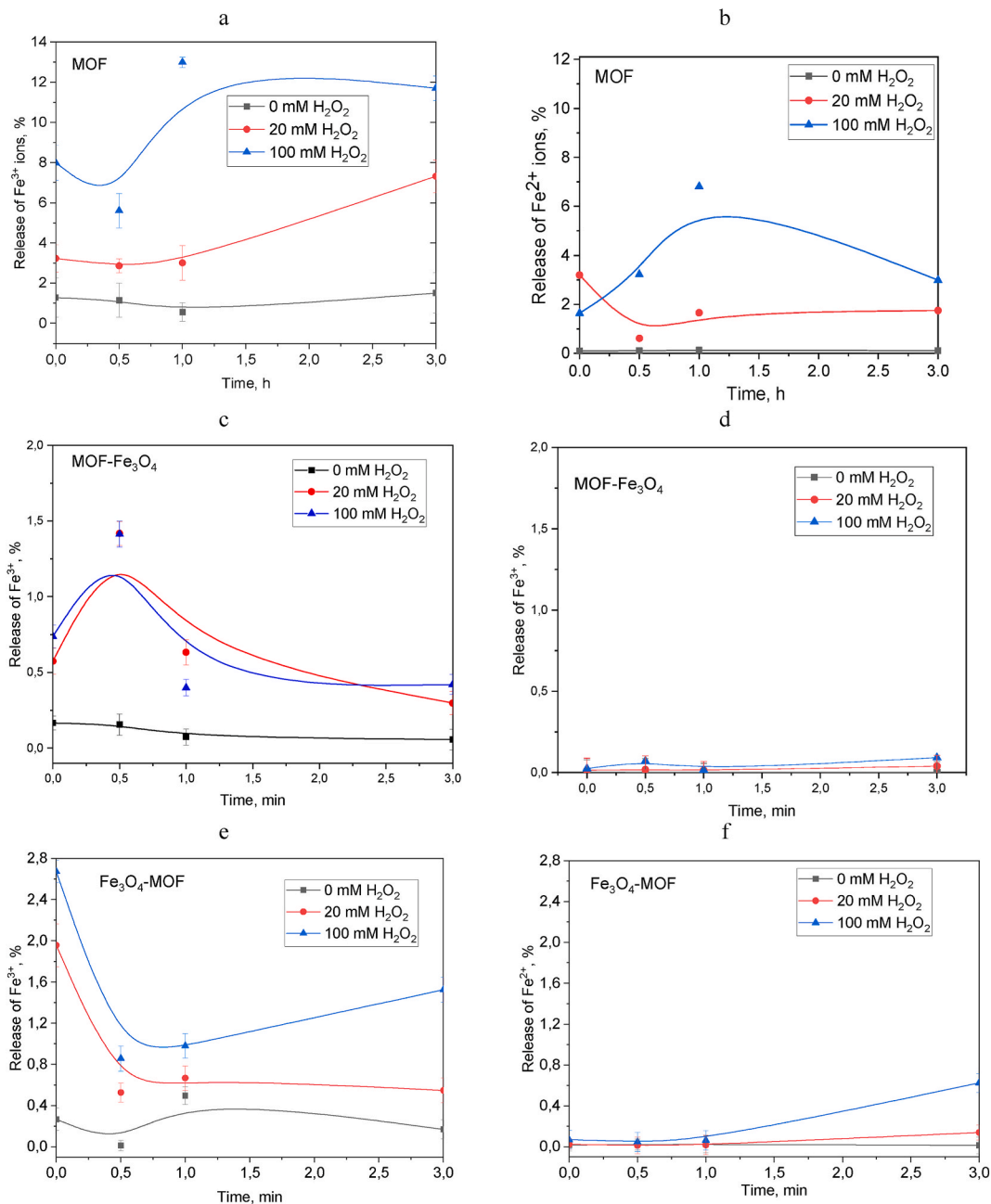


Fig. 16. Release of Fe³⁺ and Fe²⁺ from MOF (a, b), MOF-Fe₃O₄ (c, d) and Fe₃O₄-MOF (e, f) at pH 4.5.

Funding

This research was funded by Russian Science Foundation, grant number 22-73-10222. Part of analysis was supported by Austrian Academic Exchange Service (OeAD) MPC-2022-02194. Marco Reindl was trained within the frame of the PhD program in Molecular Medicine.

Data availability statement

The data is available upon request from the corresponding author.

CRediT authorship contribution statement

Lyubov Bondarenko: Writing – original draft, Project administration, Methodology, Investigation, Formal analysis, Data curation, Conceptualization. **Rose Baimuratova:** Writing – review & editing, Investigation, Formal analysis. **Marco Reindl:** Writing – review & editing, Data curation. **Verena Zach:** Writing – review & editing, Data curation. **Artur Dzeranov:** Writing – review & editing, Formal analysis, Data curation. **Denis Pankratov:** Writing – review & editing, Formal analysis, Data curation. **Kamila Kydralieva:** Writing – review & editing, Supervision, Resources, Project administration, Conceptualization. **Gulzhian Dzhardimalieva:** Writing – review & editing, Formal analysis, Data curation. **Dagmar Kolb:** Writing – review & editing, Methodology, Data curation. **Friedrich E. Wagner:** Methodology, Investigation, Data curation. **Sebastian P. Schwaminger:** Writing – review & editing, Supervision, Methodology, Funding acquisition, Conceptualization.

Declaration of competing interest

The authors declare that they have no known competing financial interests or personal relationships that could have appeared to influence the work reported in this paper.

Appendix A. Supplementary data

Supplementary data to this article can be found online at <https://doi.org/10.1016/j.heliyon.2024.e27640>.

References

- [1] M.J. Ko, S. Min, H. Hong, W. Yoo, J. Joo, Y.S. Zhang, H. Kang, D.-H. Kim, Magnetic NPs for ferroptosis cancer therapy with diagnostic imaging, *Bioact. Mater.* 32 (Feb. 2024) 66–97.
- [2] S.R. Batten, N.R. Champness, X.-M. Chen, J. Garcia-Martinez, S. Kitagawa, L. Ghrstl, M. O'Keefe, M. Paik Suh, J. Reedijk, "Terminology of metal-organic frameworks and coordination polymers (iupac recommendations 2013)," *Pure Appl. Chem.* 85 (July 2013) 1715–1724.
- [3] R.-B. Lin, S. Xiang, H. Xing, W. Zhou, B. Chen, "Exploration of porous metal-organic frameworks for gas separation and purification," *Coord. Chem. Rev.* 378 (Jan. 2019) 87–103.
- [4] I.M. Hrnicek, I. Senkova, V. Bon, I.A. Baburin, N. Brnisch, S. Raschke, J.D. Evans, S. Kaskel, Balancing mechanical stability and ultrahigh porosity in crystalline framework materials, *Angew. Chem. Int. Ed.* 57 (Sept. 2018) 13780–13783.
- [5] P. Horcajada, T. Chalati, C. Serre, B. Gillet, C. Sebrie, T. Baati, J.F. Eubank, D. Heurtaux, P. Clayette, C. Kreuz, J.-S. Chang, Y.K. Hwang, V. Marsaud, P.-N. Bories, L. Cynober, S. Gil, G. Férey, P. Couvreur, R. Gref, Porous metalorganic-framework nanoscale carriers as a potential platform for drug delivery and imaging, *Nat. Mater.* 9 (dec 2009) 172–178.
- [6] F.R.S. Lucena, L.C. de Araujo, M.d.D. Rodrigues, T.G. da Silva, V.R. Pereira, G.C. Milito, D.A. Fontes, P.J. Rolim-Neto, F.F. da Silva, S.C. Nascimento, Induction of cancer cell death by apoptosis and slow release of 5-fluoracil from metal-organic frameworks cu-btc, *Biomed. Pharmacother.* 67 (Oct. 2013) 707–713.
- [7] M. Gimenez-Marqu, T. Hidalgo, C. Serre, P. Horcajada, "Nanostructured metal-organic frameworks and their bio-related applications," *Coord. Chem. Rev.* 307 (Jan. 2016) 342–360.
- [8] H.D. Lawson, S.P. Walton, C. Chan, "Metal-organic frameworks for drug delivery: a design perspective," *ACS Appl. Mater. Interfaces* 13 (Feb. 2021) 7004–7020.
- [9] P.-H. Tong, L. Zhu, Y. Zang, J. Li, X.-P. He, T.D. James, "Metal-organic frameworks (mofs) as host materials for the enhanced delivery of biomacromolecular therapeutics," *Chem. Commun.* 57 (91) (2021) 12098–12110.
- [10] M. Sajid, Ihsanullah, Toxicity of Nanoscale Metal-Organic Frameworks in Biological Systems, 2020, pp. 383–395.
- [11] A.A. Sopianik, M.A. Kiskin, K.A. Kovalenko, D.G. Samsonenko, D.N. Dybtsev, N. Audebrand, Y. Sun, V.P. Fedin, Rational synthesis and dimensionality tuning of mofs from preorganized heterometallic molecular complexes, *Dalton Trans.* 48 (11) (2019) 3676–3686.
- [12] N. Stock, S. Biswas, Synthesis of metal-organic frameworks (mofs): routes to various mof topologies, morphologies, and composites, *Chem. Rev.* 112 (Nov. 2011) 933–969.
- [13] S. Jabarian, A. Ghaffarinejad, Electrochemical synthesis of nibt metal organic framework thin layer on nickel foam: an efficient electrocatalyst for the hydrogen evolution reaction, *J. Inorg. Organomet. Polym. Mater.* 29 (Feb. 2019) 1565–1574.
- [14] D. Chen, J. Zhao, P. Zhang, S. Dai, "Mechanochemical synthesis of metal-organic frameworks," *Polyhedron* 162 (Apr. 2019) 59–64.
- [15] W. Yuan, T. Fri, D. Apperley, S. James, "High reactivity of metal-organic frameworks under grinding conditions: parallels with organic molecular materials," *Angew. Chem. Int. Ed.* 49 (May 2010) 3916–3919.
- [16] G. Sargazi, D. Afzali, A. Mostafavi, "An efficient and controllable ultrasonic-assisted microwave route for flower-like ta(v)-mof nanostructures: preparation, fractional factorial design, dft calculations, and high-performance n2 adsorption," *J. Porous Mater.* 25 (Feb. 2018) 1723–1741.
- [17] N.A. Khan, S.H. Jung, Synthesis of metal-organic frameworks (mofs) with microwave or ultrasound: rapid reaction, phase-selectivity, and size reduction, *Coord. Chem. Rev.* 285 (Feb. 2015) 11–23.
- [18] E. Burgaz, A. Erciyes, M. Andac, O. Andac, Synthesis and characterization of nano-sized metal organic framework-5 (mof-5) by using consecutive combination of ultrasound and microwave irradiation methods, *Inorg. Chim. Acta.* 485 (Jan. 2019) 118–124.
- [19] Q. Xia, H. Wang, B. Huang, X. Yuan, J. Zhang, J. Zhang, L. Jiang, T. Xiong, G. Zeng, State-of-the-art advances and challenges of iron-based metal organic frameworks from attractive features, synthesis to multifunctional applications, *Small* 15 (Dec. 2018).
- [20] D.-W. Wang, D. Su, Heterogeneous nanocarbon materials for oxygen reduction reaction, *Energy & Environmental Science* 7 (2) (2014) 576.
- [21] C. Gao, S. Chen, X. Quan, H. Yu, Y. Zhang, Enhanced fenton-like catalysis by iron-based metal organic frameworks for degradation of organic pollutants, *J. Catal.* 356 (Dec. 2017) 125–132.
- [22] J. He, Y. Zhang, X. Zhang, Y. Huang, Highly efficient fenton and enzyme-mimetic activities of nh2-mil-88b(fe) metal organic framework for methylene blue degradation, *Sci. Rep.* 8 (Mar. 2018).
- [23] S.G. Guillen, J. Parres-Gold, A. Ruiz, E. Lucsik, B. Dao, T.K.L. Hang, M. Chang, A.O. Garcia, Y. Wang, F. Tian, "ph-responsive metal-organic framework thin film for drug delivery," *Langmuir* 38 (Dec. 2022) 16014–16023.
- [24] N. Thomas, D.D. Dionysiou, S.C. Pillai, Heterogeneous fenton catalysts: a review of recent advances, *J. Hazard Mater.* 404 (Feb. 2021) 124082.
- [25] M.F. Dapaah, Q. Niu, Y.-Y. Yu, T. You, B. Liu, L. Cheng, "Efficient persistent organic pollutant removal in water using mil-metal-organic framework driven fenton-like reactions: a critical review," *Chem. Eng. J.* 431 (Mar. 2022) 134182.

- [26] L. Zheng, Y. Gu, B. Hua, J. Fu, F. Li, Hierarchical porous melamine sponge@mil-101-fe-nh2 composite as fenton-like catalyst for efficient and rapid tetracycline hydrochloride removal, *Chemosphere* 307 (Nov. 2022) 135728.
- [27] N.A. Khan, Z. Hasan, S.H. Jung, Adsorptive removal of hazardous materials using metal-organic frameworks (mofs): a review, *J. Hazard Mater.* 244b7j“245 (Jan. 2013) 444–456.
- [28] Q. Wu, H. Yang, L. Kang, Z. Gao, F. Ren, Fe-based metal-organic frameworks as fenton-like catalysts for highly efficient degradation of tetracycline hydrochloride over a wide pH range: acceleration of fe(ii)/fe(iii) cycle under visible light irradiation, *Appl. Catal. B Environ.* 263 (Apr. 2020) 118282.
- [29] C. Yang, G. Xu, Q. Liu, Adsorption and heterogenous fenton-like reactivity of nh2-mil-88b towards toxic dyes removal, *Colloids Surf. A Physicochem. Eng. Asp.* 677 (Nov. 2023) 132405.
- [30] Y. Qiu, Y. Cao, W. Cao, Y. Jia, N. Lu, The application of ferroptosis in diseases, *Pharmacol. Res.* 159 (Sept. 2020) 104919.
- [31] H.-f. Yan, T. Zou, Q.-z. Tuo, S. Xu, H. Li, A.A. Belaidi, P. Lei, Ferroptosis: mechanisms and links with diseases, in: *Signal Transduction and Targeted Therapy*, vol. 6, Feb. 2021.
- [32] S. Lee, S. An, Y.C. Ryu, S.H. Seo, S. Park, M.J. Lee, S. Cho, K. Choi, Adhesive hydrogel patch-mediated combination drug therapy induces regenerative wound healing through reconstruction of regenerative microenvironment, *Adv. Healthcare Mater.* 12 (Mar. 2023).
- [33] A.-N. Cho, Y. Jin, Y. An, J. Kim, Y.S. Choi, J.S. Lee, J. Kim, W.-Y. Choi, D.-J. Koo, W. Yu, G.-E. Chang, D.-Y. Kim, S.-H. Jo, J. Kim, S.-Y. Kim, Y.-G. Kim, J.Y. Kim, N. Choi, E. Cheong, Y.-J. Kim, H.S. Je, H.-C. Kang, S.-W. Cho, Microfluidic device with brain extracellular matrix promotes structural and functional maturation of human brain organoids, *Nat. Commun.* 12 (Aug) (2021).
- [34] C. Chen, Y. Wang, H. Zhang, H. Zhang, W. Dong, W. Sun, Y. Zhao, Responsive and self-healing structural color supramolecular hydrogel patch for diabetic wound treatment, *Bioact. Mater.* 15 (Sept. 2022) 194–202.
- [35] Z. Ye, W. Zhang, S. Lanzalaco, L. Zhao, I. SirfOs, P. Xia, J. Zhai, Q. He, Ultra-uniform mil-88b(fe)/fe3s4 hybrids engineered by partial sulfidation to boost catalysis in electro-fenton treatment of micropollutants: experimental and mechanistic insights, *Chem. Eng. J.* 455 (Jan. 2023) 140757.
- [36] M.U. Akbar, S. Khattak, M.I. Khan, U.A.K. Saddozai, N. Ali, A.F. AlAsmari, M. Zaheer, M. Badar, A ph-responsive bi-mil-88b mof coated with folic acid-conjugated chitosan as a promising nanocarrier for targeted drug delivery of 5-fluorouracil, *Front. Pharmacol.* 14 (Sept) (2023).
- [37] A. Samui, A.R. Chowdhuri, T.K. Mahto, S.K. Sahu, Fabrication of a magnetic nanoparticle embedded nh2-mil-88b mof hybrid for highly efficient covalent immobilization of lipase, *RSC Adv.* 6 (71) (2016) 66385–66393.
- [38] O.M. Yaghi, M. OвТМKeeffe, N.W. Ockawig, H.K. Chae, M. Eddaoudi, J. Kim, Reticular synthesis and the design of new materials, *Nature* 423 (June 2003) 705–714.
- [39] M. Zhang, M. Bosch, T. Gentle III, H.-C. Zhou, “Rational design of metals”organic frameworks with anticipated porosities and functionalities,” *CrystEngComm* 16 (20) (2014) 4069–4083.
- [40] R.K. Baimuratova, V.A. Zhinzhiro, I.E. Uflyand, A.I. Dmitriev, M.V. Zhidkov, N.S. Ovanesyan, G.D. Kugabaeva, G.I. Dzhardimalieva, “Low-temperature synthesis of metals”organic coordination polymers based on oxo-centered iron complexes: magnetic and adsorption properties,” *Russ. J. Phys. Chem. A* 97 (Apr. 2023) 735–748.
- [41] L. Peng, M. Asgari, P. Mievill, P. Schouwink, S. Bulut, D.T. Sun, Z. Zhou, P. Pattison, W. van Beek, W.L. Queen, Using predefined msb3/sub(sub3/sub-o) clusters as building blocks for an isostructural series of metalorganic frameworks, *ACS Applied Materials & Interfaces* 9 (2017) 23957–23966, jul.
- [42] S. SurblГ©, C. Serre, C. Mellot-Draznieks, F. Millange, G. FrОrey, A new isorectical class of metal-organic-frameworks with the mil-88 topology, *Chem. Commun.* 3 (2006) 284–286.
- [43] W.C. Elmore, Ferromagnetic colloid for studying magnetic structures, *Phys. Rev.* 54 (aug 1938) 309–310.
- [44] S. Schwaminger, C. Syhr, S. Berensmeier, Controlled synthesis of magnetic iron oxide NPs: magnetite or maghemite? *Crystals* 10 (mar 2020) 214.
- [45] D. Bara, E.G. Meekel, I. Pakamore, C. Wilson, S. Ling, R.S. Forgan, Exploring and expanding the fe-terephthalate metalorganic framework phase space by coordination and oxidation modulation, *Mater. Horiz.* 8 (12) (2021) 3377–3386.
- [46] R. Pallach, J. Keupp, K. Terlinden, L. Frenzel-Beyme, M. KloБ, A. Machalica, J. Kotschy, S.K. Vasa, P.A. Chater, C. Sternemann, M.T. Wharmby, R. Linsler, R. Schmid, S. Henke, Frustrated flexibility in metal-organic frameworks, *Nat. Commun.* 12 (jul 2021).
- [47] C. Mellot-Draznieks, C. Serre, S. SurblГ©, N. Audebrand, G. FГrey, Very large swelling in hybrid frameworks:0.167em a combined computational and powder diffraction study, *J. Am. Chem. Soc.* 127 (oct 2005) 16273–16278.
- [48] W. Kim, C.-Y. Suh, S.-W. Cho, K.-M. Roh, H. Kwon, K. Song, I.-J. Shon, A new method for the identification and quantification of magnetitemaghemite mixture using conventional x-ray diffraction technique, *Talanta* 94 (may 2012) 348–352.
- [49] H. He, Y. Wang, J. Li, S. Jiang, S. Sidra, W. Gong, Y. Tang, Y. Hu, R. Wei, D. Yang, X. Li, Z. Zhao, Confined conductive and light-adsorbed network in metal organic frameworks (MIL-88b(fe)) with enhanced photo-fenton catalytic activity for sulfamethoxazole degradation, *Chem. Eng. J.* 427 (jan 2022) 131962.
- [50] H.T. Varghese, C.Y. Panicker, D. Philip, K. Sreevalsan, V. Anithakumary, IR, Raman and SERS spectra of disodium terephthalate, *Spectrochim. Acta Mol. Biomol. Spectrosc.* 68 (nov 2007) 817–822.
- [51] J. Arenas, J. Marcos, Infrared and Raman spectra of phthalic, isophthalic and terephthalic acids, *Spectrochim. Acta Mol. Spectrosc.* 36 (jan 1980) 1075–1081.
- [52] K. Nakamoto, Infrared Andscpr/scpaman Spectra of Inorganic and Coordination Compounds, dec 2001.
- [53] G.-T. Vuong, M.-H. Pham, T.-O. Do, Direct synthesis and mechanism of the formation of mixed metal fe2ni-MIL-88b, *CrystEngComm* 15 (45) (2013) 9694.
- [54] S.P. Schwaminger, D. Bauer, P. Fraga-Garcá, F.E. Wagner, S. Berensmeier, Oxidation of magnetite NPs: impact on surface and crystal properties, *CrystEngComm* 19 (2) (2017) 246–255.
- [55] R.L. Rebodos, P.J. Vikesland, Effects of oxidation on the magnetization of nanoparticulate magnetite, *Langmuir* 26 (sep 2010) 16745–16753.
- [56] Y.E. Mendili, J.-F. Bardeau, N. Randrianantoandro, F. Grasset, J.-M. Grenèche, Insights into the mechanism related to the phase transition from -fesub2/subosub3/sub to -fesub2/subosub3/sub NPs induced by thermal treatment and laser irradiation, *J. Phys. Chem. C* 116 (oct 2012) 23785–23792.
- [57] G.V. Jacintho, P. Corio, J.C. Rubim, Surface-enhanced Raman spectra of magnetic NPs adsorbed on a silver electrode, *J. Electroanal. Chem.* 603 (may 2007) 27–34.
- [58] G. Deacon, F. Huber, R. Phillips, Diagnosis of the nature of carboxylate coordination from the direction of shifts of carbono—oxygen stretching frequencies, *Inorg. Chim. Acta.* 104 (oct 1985) 41–45.
- [59] H. Namduri, S. Nasrazadani, Quantitative analysis of iron oxides using fourier transform infrared spectrophotometry, *Corrosion Sci.* 50 (sep 2008) 2493–2497.
- [60] M. Ishii, M. Nakahira, T. Yamanaka, Infrared absorption spectra and cation distributions in (mn, fe)3o4, *Solid State Commun.* 11 (jul 1972) 209–212.
- [61] M. Sanselme, J.-M. Grenèche, M. Riou-Cavellec, G. FГrey, The first ferric carboxylate with a three-dimensional hybrid open-framework (MIL-82): its synthesis, structure, magnetic behavior and study of its dehydration by mI”ssbauer spectroscopy, *Solid State Sci.* 6 (aug 2004) 853–858.
- [62] Y. Yue, H. Arman, Z.J. Tonzetch, B. Chen, Air-free synthesis of a ferrous metal-organic framework featuring HKUST-1 structure and its mI”ssbauer spectrum, *Zeitschrift fГr anorganische und allgemeine Chemie* 645 (may 2019) 797–800.
- [63] D.A. Pankratov, MI”ssbauer study of oxo derivatives of iron in the fe2o3-na2o2 system, *Inorg. Mater.* 50 (dec 2013) 82–89.
- [64] A. Laurikeas, J. Barkauskas, J. Reklaitis, G. Niaura, D. Baltrunas, A. Kareiva, Formation peculiarities of iron (III) acetate: potential precursor for iron metal-organic frameworks (MOFs), *Lith. J. Phys.* 56 (apr 2016).
- [65] A. Fateeva, N. Guillou, T. Devic, Insightful contribution of 57fe mОssbauer spectrometry (and of jean-marc grenèche) to the field of iron metal organic frameworks, *J. Mater. Res.* 38 (2022) 1007–1018.
- [66] C.E. Johnson, Characterization of magnetic materials by mI”ssbauer spectroscopy, *J. Phys. Appl. Phys.* 29 (sep 1996) 2266–2273.
- [67] D.A. Pankratov, M.M. Anuchina, F.M. Spiridonov, G.G. Krivtsov, Fe3 o4 NPs synthesized in the presence of natural polyelectrolytes, *Crystallogr. Rep.* 65 (may 2020) 393–397.
- [68] F.J. Berry, S. Skinner, M.F. Thomas, MI”ssbauer spectroscopic examination of a single crystal of, *J. Phys. Condens. Matter* 10 (jan 1998) 215–220.
- [69] D.H. Jones, K.K.P. Srivastava, Many-state relaxation model for the mI”ssbauer spectra of superparamagnets, *Phys. Rev. B* 34 (dec 1986) 7542–7548.
- [70] A. Dzeranov, L. Bondarenko, D. Pankratov, G. Dzhardimalieva, S. Jorobekova, D. Saman, K. Kydraliev, Impact of silica-modification and oxidation on the crystal structure of magnetite NPs, *Magnetochemistry* 9 (18) (jan 2023).

- [71] H. Hah, S. Gray, C. Johnson, J. Johnson, V. Kolesnichenko, P. Kucheryavy, G. Goloverda, Mössbauer spectroscopy of superparamagnetic Fe₃O₄ NPs, *J. Magn. Magn. Mater.* 539 (dec 2021) 168382.
- [72] D.A. Pankratov, M.M. Anuchina, Nature-inspired synthesis of magnetic non-stoichiometric Fe₃O₄ NPs by oxidative in situ method in a humic medium, *Mater. Chem. Phys.* 231 (June 2019) 216–224.
- [73] L.S. Bondarenko, D.A. Pankratov, A.A. Dzeranov, G.I. Dzhardimalieva, A.N. Streltsova, M. Zarrelli, K.A. Kydralieva, A simple method for quantification of nonstoichiometric magnetite NPs using conventional x-ray diffraction technique, *Mendelev Commun.* 32 (Sept. 2022) 642–644.
- [74] Y. Gao, S. Yan, Y. He, Y. Fan, L. Zhang, J. Ma, R. Hou, L. Chen, J. Chen, A photo-fenton self-cleaning membrane based on NH₂-MIL-88b(Fe) and graphene oxide to improve dye removal performance, *J. Membr. Sci.* 626 (may 2021) 119192.
- [75] Y. Wang, Z. Zhong, Y. Muhammad, H. He, Z. Zhao, S. Nie, Z. Zhao, Defect engineering of NH₂-MIL-88b(Fe) using different monodentate ligands for enhancement of photo-fenton catalytic performance of acetamiprid degradation, *Chem. Eng. J.* 398 (oct 2020) 125684.
- [76] M. Ahmad, X. Quan, S. Chen, H. Yu, Tuning Lewis acidity of MIL-88b-Fe with mix-valence coordinatively unsaturated iron centers on ultrathin Ti₃C₂ nanosheets for efficient photo-fenton reaction, *Appl. Catal. B Environ.* 264 (may 2020) 118534.
- [77] L. Bondarenko, E. Illés, E. Tombácz, G. Dzhardimalieva, N. Golubeva, O. Tushavina, Y. Adachi, K. Kydralieva, Fabrication, microstructure and colloidal stability of humic acids loaded Fe₃O₄/APTES nanosorbents for environmental applications, *Nanomaterials* 11 (may 2021) 1418.
- [78] A. Kolhatkar, A. Jamison, D. Litvinov, R. Willson, T. Lee, Tuning the magnetic properties of NPs, *Int. J. Mol. Sci.* 14 (jul 2013) 15977–16009.
- [79] H.-C. Roth, S.P. Schwaminger, M. Schindler, F.E. Wagner, S. Berensmeier, Influencing factors in the CO-precipitation process of superparamagnetic iron oxide nano particles: a model based study, *J. Magn. Magn. Mater.* 377 (mar 2015) 81–89.
- [80] D. Yoo, C. Lee, B. Seo, Y. Piao, One pot synthesis of amine-functionalized and angular-shaped superparamagnetic iron oxide NPs for MR/fluorescence bimodal imaging application, *RSC Adv.* 7 (21) (2017) 12876–12885.
- [81] S. Laurent, D. Forge, M. Port, A. Roch, C. Robic, L.V. Elst, R.N. Muller, Magnetic iron oxide NPs: synthesis, stabilization, vectorization, physicochemical characterizations, and biological applications, *Chem. Rev.* 108 (jun 2008) 2064–2110.
- [82] F. Wang, G.M. Pauletti, J. Wang, J. Zhang, R.C. Ewing, Y. Wang, D. Shi, Dual surface-functionalized Janus nanocomposites of polystyrene/Fe₃O₄@SiO₂ for simultaneous tumor cell targeting and stimulus-induced drug release, *Adv. Mater.* 25 (May 2013) 3485–3489.
- [83] M.S. Moorthy, Y. Oh, S. Bharathiraja, P. Manivasagan, T. Rajarathinam, B. Jang, T.T. Vy Phan, H. Jang, J. Oh, Synthesis of amine-polyglycidol functionalised Fe₃O₄@SiO₂ nanocomposites for magnetic hyperthermia, pH-responsive drug delivery, and bioimaging applications, *RSC Adv.* 6 (111) (2016) 110444–110453.
- [84] S. Kayal, R. Ramanujan, Doxorubicin loaded pva coated iron oxide NPs for targeted drug delivery, *Mater. Sci. Eng. C* 30 (Apr. 2010) 484–490.
- [85] M. Huo, L. Wang, Y. Chen, J. Shi, Tumor-selective catalytic nanomedicine by nanocatalyst delivery, *Nat. Commun.* 8 (aug 2017).
- [86] C.A. Gorski, M.M. Scherer, Determination of nanoparticulate magnetite stoichiometry by Mössbauer spectroscopy, acidic dissolution, and powder x-ray diffraction: a critical review, *Am. Mineral.* 95 (June 2010) 1017–1026.
- [87] A.M. Jubb, H.C. Allen, Vibrational spectroscopic characterization of hematite, maghemite, and magnetite thin films produced by vapor deposition, *ACS Appl. Mater. Interfaces* 2 (Sept. 2010) 2804–2812.
- [88] I. Chamritski, G. Burns, Infrared- and Raman-active phonons of magnetite, maghemite, and hematite: a computer simulation and spectroscopic study, *J. Phys. Chem. B* 109 (Feb. 2005) 4965–4968.
- [89] C. Gao, S. Chen, X. Quan, H. Yu, Y. Zhang, Enhanced Fenton-like catalysis by iron-based metal organic frameworks for degradation of organic pollutants, *J. Catal.* 356 (dec 2017) 125–132.
- [90] I. Bezverkhy, G. Weber, J.-P. Bellat, Degradation of fluoride-free MIL-100(Fe) and MIL-53(Fe) in water: effect of temperature and pH, *Microporous Mesoporous Mater.* 219 (Jan. 2016) 117–124.